

# Sensitivity of firing rate to input fluctuations depends on time scale separation between fast and slow variables in single neurons

Brian Nils Lundstrom · Michael Famulare ·  
Larry B. Sorensen · William J. Spain ·  
Adrienne L. Fairhall

Received: 20 August 2008 / Revised: 11 December 2008 / Accepted: 6 February 2009 / Published online: 8 April 2009  
© Springer Science + Business Media, LLC 2009

**Abstract** Neuronal responses are often characterized by the firing rate as a function of the stimulus mean, or the  $f-I$  curve. We introduce a novel classification of neurons into Types A, B<sup>-</sup>, and B<sup>+</sup> according to how  $f-I$  curves are modulated by input fluctuations. In Type A neurons, the  $f-I$  curves display little sensitivity to input fluctuations when the mean current is large. In contrast, Type B neurons display sensitivity to fluctuations throughout the entire range of input means. Type B<sup>-</sup> neurons do not fire repetitively for any constant input, whereas Type B<sup>+</sup> neurons do. We show that Type B<sup>+</sup> behavior results from a separation of time scales between a slow and fast variable. A voltage-dependent time constant for the recovery variable can facilitate sensitivity to input fluctuations. Type B<sup>+</sup> firing rates can be approximated using a simple “energy barrier” model.

**Keywords** Noise · Gain ·  $f-I$  curve · Stimulus fluctuations · Single neuron · Time scales · Dynamical systems · Phase portrait · Hodgkin-Huxley · Slow adaptation · Slow AHP

---

Action Editor: Bard Ermentrout

---

B. N. Lundstrom (✉) · W. J. Spain · A. L. Fairhall  
Department of Physiology and Biophysics,  
University of Washington,  
Seattle, WA 98195, USA  
e-mail: lundbr@u.washington.edu

M. Famulare · L. B. Sorensen  
Department of Physics, University of Washington,  
Seattle, WA 98195, USA

W. J. Spain  
Neurology Section,  
Veterans Affairs Puget Sound Health Care System,  
1660 South Columbian Way,  
Seattle, WA 98108, USA

## 1 Introduction

The output of a neuron can be described in terms of precise spike timing or the mean firing rate (Shadlen and Newsome 1994; Konig et al. 1996; VanRullen et al. 2005). Both of these coding strategies convey information, possibly distinct, about the stimulus (Fairhall et al. 2001; Lundstrom and Fairhall 2006). Here, we focus on how the mean firing rate of a single-compartment neuron encodes the statistical properties of current inputs, which we approximate as filtered Gaussian noise (Destexhe et al. 2001, 2003; Moreno et al. 2002; for discussion, see Rauch et al. 2003; Richardson 2004; Rudolph and Destexhe 2005, 2006).

While firing rate generally increases with stimulus mean, the slope of the firing rate to input current ( $f-I$ ) curve can be altered by the variance of the fluctuating input. This can be seen as a type of gain control (Chance et al. 2002; Fellous et al. 2003; Rauch et al. 2003; Higgs et al. 2006; Arsiero et al. 2007; Lundstrom et al. 2008), whereby the strength of background fluctuations modulates the response to the mean. More generally, the firing rate varies with, and thereby encodes, both mean and variance, and the sensitivity to one or the other can be interpreted as conferring on the neuron integrator-like or differentiator-like properties, respectively (Higgs et al. 2006; Lundstrom et al. 2008). For example, the average firing rate of layer 5 pyramidal neurons of the sensorimotor cortex recorded *in vitro* varies with input mean but depends less strongly on input variance (Chance et al. 2002; Rauch et al. 2003); these neurons can be thought of as integrators. The firing rates of other neurons, e.g. from the rat prefrontal cortex, are more sensitive to changes of input variance (Fellous et al. 2003; Arsiero et al. 2007) and can be classified as differentiators, or coincidence detectors, where this sensitivity to transients

can be facilitated by mechanisms underlying spike rate adaptation (Benda et al. 2005; Higgs et al. 2006; Prescott et al. 2006). However, a strict dichotomy between integrator and differentiator is artificial. Plotting  $f$ - $I$  curves for a number of examples of recent *in vitro* data [Fig. 1(a)], it is clear that the firing rate is often sensitive to both input mean and variance, and that sensitivity varies over the neuron's dynamic range.

To what extent is this range of behavior captured by standard single-compartment model neurons? We show responses to similar stimuli for a variety of conventional model neurons in Fig. 1(b). None of the models reproduce the firing rate sensitivity of some *in vitro* neurons to input fluctuations above rheobase, the lowest DC current for which the neuron fires repetitively. For example, even if slow adaptation currents are added to the leaky-integrate-and-fire neuron, at high enough mean inputs the interspike

interval equals the refractory period, yielding a firing rate that is insensitive to input fluctuations. What, then, is necessary for single-compartment model neurons to show noise sensitivity above rheobase?

To provide a framework within which to place these and previous results, we categorize neurons according to their  $f$ - $I$  curves into three classes: Types A, B+, and B-. These types are distinct from those of Hodgkin's three classes (Hodgkin 1948; Rinzel and Ermentrout 1998; Gerstner and Kistler 2002; Izhikevich 2007), which focus on the bifurcations of neurons in response to noiseless currents. The  $f$ - $I$  curves of Type A neurons show little sensitivity to input fluctuations above rheobase, as is the case for many standard single-compartment model neurons [Fig. 1(b)]. On the other hand,  $f$ - $I$  curves from Type B neurons display sensitivity to input fluctuations throughout the neuron's dynamic range. We parse Type B into two categories depending on whether or

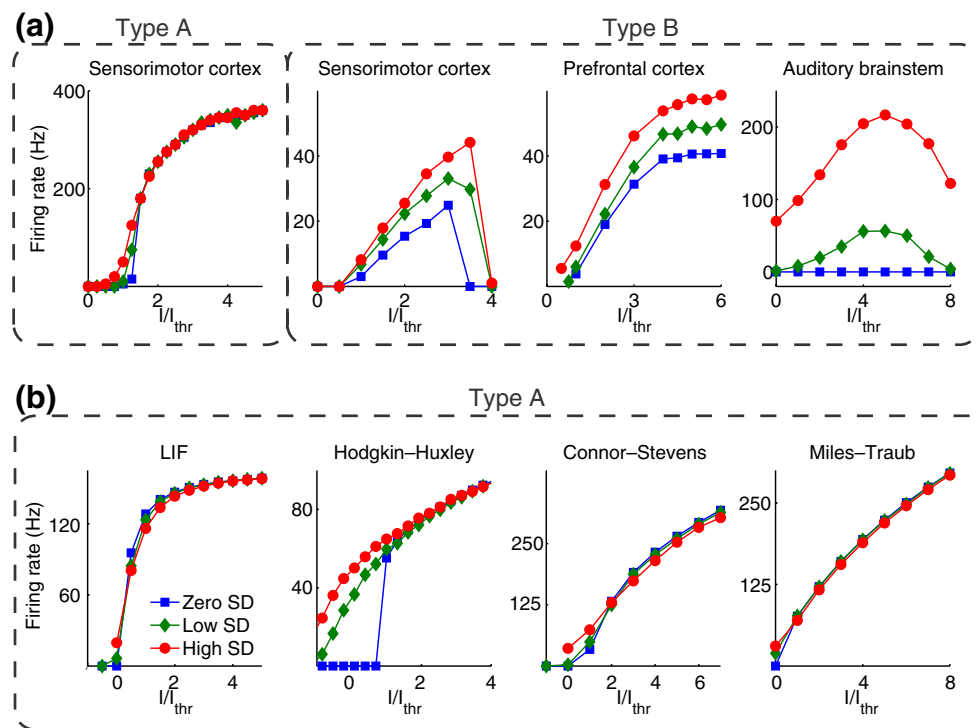


**Fig. 1** The firing rates of *in vitro* neurons (*top row*) can display greater sensitivity to noise than those of conventional model neurons (*bottom row*). Type A neurons show little sensitivity to input fluctuations for large input means, while Type B neurons are sensitive throughout their physiological range. **(a)** Mean firing rate is plotted as a function of mean input current, where different traces represent different input SD with circles as highest input SD. From left to right,  $SD=[0, 0.7, 1.3]$ ,  $[0, 0.5, 1]$ ,  $[0.25, 0.75, 1.5]$ , and  $[0, 1, 2]$  in units of  $I_{thr}$ , which was estimated to be the rheobase, or minimum zero-noise current needed to elicit spiking. From left to right  $I_{thr}=300, 400, 200$ , and  $200$  pA. From left to right, the first three neurons are from the neocortex (fast-spiking interneuron and two regular spiking pyramidal neurons) and the fourth is from the auditory brainstem (nucleus laminaris). Data from the sensorimotor cortex and auditory brainstem

are courtesy of Matthew Higgs (Higgs et al. 2006), and data from the prefrontal cortex are courtesy of Michele Giugliano (Arsiero et al. 2007). **(b)** The mean firing rate of many single-compartment model neurons is insensitive to input SD for high input currents (i.e. above rheobase). From left to right,  $SD=[0, 0.5, 1]$ ,  $[0, 0.5, 1]$ ,  $[0, 1.5, 3]$ , and  $[0, 1, 2]$  in units of  $I_{thr}$  with  $I_{thr}=40, 65, 100$ , and  $25$  nA/mm<sup>2</sup> respectively. The leaky integrate-and-fire neuron is a standard one-dimensional model often used for network modeling (Dayan and Abbott 2001), the classic Hodgkin-Huxley neuron models the squid giant axon (Hodgkin and Huxley 1952), the Connor-Stevens model is a prototypical Class I model based on a gastropod neuron (Connor and Stevens 1971), and the Miles-Traub model is based on hippocampal neurons (Ermentrout 1998)

not they fire repetitively to noiseless input. Type B- models do not fire repetitively unless noise is present in the input, while Type B+ models can. The transition from Type A to B- behavior has been explored previously (Lundstrom et al. 2008). We explore the causes leading to Type B+ behavior. We show how a separation of time scales between activation and recovery from spiking, such as might be induced by a voltage-dependent time constant for the recovery variable, promotes sensitivity to input fluctuations in low dimensional neuron models.

## 2 Methods

The two-dimensional model of Fig. 2 is described by the following equations, which are derived from the standard four-dimensional Hodgkin–Huxley (HH) model (Hodgkin and Huxley 1952; Koch 1999; Dayan and Abbott 2001; Gerstner and Kistler 2002) by eliminating the time dependence of  $m$  and letting  $h$  linearly depend on  $n$ , as in previous work (Rush and Rinzel 1995; Gerstner and Kistler 2002; Izhikevich 2007); we then altered the kinetics and conductances:

$$\begin{aligned} C \frac{dV}{dt} &= -G_{Na}m^3h(V - E_{Na}) - G_Kn^4(V - E_K) - G_{Leak}(V - E_{Leak}) + I \\ \tau \frac{dn}{dt} &= n_\infty - n \end{aligned} \tag{1}$$

where

$$\begin{aligned} m_\infty &= 1/(1 + \exp((-40 - V)/k_m)) \\ h &= 0.89 - 1.1n \\ n_\infty &= 1/(1 + \exp((V_n - V)/k_n)) \end{aligned}, \tag{2}$$

with parameters  $C=1$  nF/mm<sup>2</sup>,  $G_{Na}=50$  mS/cm<sup>2</sup>,  $G_K=36$  mS/cm<sup>2</sup>,  $G_{Leak}=5$  mS/cm<sup>2</sup>,  $E_{Na}=50$  mV,  $E_K=-77$  mV,  $E_{Leak}=-54$  mV,  $k_m=7$ ,  $V_n=-45$ ,  $k_n=15$ , and  $\tau=5$  or 100 ms

(except as noted). This 2D model loses stability via a subcritical Hopf bifurcation, and can be termed a Class II model (Rinzel and Ermentrout 1998; Izhikevich 2007). With modified parameters,  $G_{Leak}=15$  ms/cm<sup>2</sup>,  $V_n=-30$  mV, and  $k_n=5$ , the model is Class I and loses stability via a saddle-node on invariant circle bifurcation. Bifurcation analyses were done using XPPAUT (developed by Bard Ermentrout). When  $\tau$  was not constant, its voltage dependence was taken to be (Izhikevich 2007):

$$\tau = C_{Base} + C_{Amp} \exp\left(-\frac{(V_{max} - V)^2}{\Delta^2}\right), \tag{3}$$

with the parameters  $C_{Base}$ ,  $C_{Amp}$ ,  $V_{max}$ , and  $\Delta$ . For models of a similar form, see Izhikevich (2007). To implement slow sodium channel inactivation, an extra gating variable  $s$  was added to the sodium current so that it became:

$$I_{Na} = G_{Na}m^3hs(V - E_{Na}) \tag{4}$$

This sodium current was incorporated into the previous Class I 2D HH model. The dynamics of the variables  $n$  and  $h$  remained unchanged except that  $\tau=3$  ms. The slower gate  $s$  was identical to  $h$  except that its time constant was governed by Eq. (3) with parameters  $C_{Base}=50$  ms,  $C_{Amp}=2,000$  ms,  $V_{max}=-40$  mV and  $\Delta=5$  mV.

Importantly for this study, input fluctuations were fast compared to the dynamics of spike recovery and time between spikes. The external input current  $I$  to the neuron was 1-ms exponentially filtered Gaussian noise (i.e. equivalent to an Ornstein–Uhlenbeck process) with the means and standard deviations as specified. Results were qualitatively identical with a 5-ms filter. Model equations were integrated using a fourth-order Runge–Kutta solver with a 0.02 ms fixed time step. Spikes were counted as upward voltage crossings at  $-20$  mV if the mean of the previous 1 ms of voltages was less than  $-40$  mV.

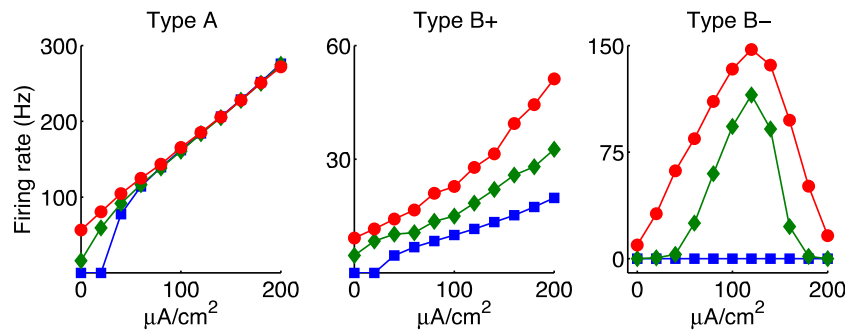


**Fig. 2** A two-dimensional modified and reduced Hodgkin-Huxley (HH) model neuron can show all three types of behavior. Type A is similar to the standard HH model and is insensitive to input SD for high currents. In contrast, Type B+ is sensitive to input SD throughout the dynamic range and fires repetitively to inputs with SD=0. Type

B- models never fire repetitively when input SD=0 and never undergo a bifurcation from stable fixed point to limit cycle. For the three models,  $G_{Na}$  and  $\tau$  were [50, 50, 15] mS/cm<sup>2</sup> and [5, 100, 5] ms, respectively. Input SD was [0, 10, 20] μA/cm<sup>2</sup>. Other parameters were as given in the Section 2

### 3 Results

Many single-compartmental biophysical model neurons, implemented with their standard parameters, display  $f$ - $I$  curves best described as Type A [Fig. 1(b)]: their firing rates are not sensitive to input fluctuations above rheobase. Here, we are interested in model neurons that display sensitivity to noise above rheobase until depolarization block, which we have called Type B. We subclassify Type B neurons as Type B<sup>-</sup> when they do not fire repetitively to noiseless current regardless of its magnitude, and Type B<sup>+</sup> if they do for some magnitude. In previous work (Lundstrom et al. 2008), we demonstrated that the alteration of a model's conductance ratio, e.g.  $G_{Na}/G_K$ , can lead to Type B<sup>-</sup>  $f$ - $I$  curves. This behavior is generated by neuronal dynamical systems with fixed points that remain stable regardless of input mean. Thus, these neurons never fire repetitively at steady state in response to noiseless input. We focus here on Type B<sup>+</sup> neurons whose firing rates are sensitive to input fluctuations throughout the dynamic range and which can fire repetitively at steady state to noiseless input.

#### 3.1 2D model demonstrating three types of $f$ - $I$ curves

We begin with a two-dimensional model, similar to the Hodgkin–Huxley neuron, that can demonstrate three types of  $f$ - $I$  curves: Type A, B<sup>+</sup>, and B<sup>-</sup> (Fig. 2). We wish to identify the specific characteristics of the differential equations describing the neuronal dynamics that lead to

the generation of Type A vs. B<sup>+</sup> behavior. For 2D dynamical systems, these characteristics can be explored geometrically using phase portraits. To do this, we reduced the standard 4D HH model to two dimensions by eliminating the time dependence of  $m$  and letting  $h$  linearly depend on  $n$  (Izhikevich 2007); we slightly altered the kinetics and conductances. We then examined 2D model trajectories in the phase plane for each of the neuron types.

Two-dimensional dynamical systems can be analyzed by examining a phase portrait, which is a plot of one dynamical variable against the other (Strogatz 1994; Gerstner and Kistler 2002; Izhikevich 2007). In this case, the model has a fast positive feedback variable  $V$  and a slow negative feedback variable  $n$ .  $V$  is the model's membrane voltage, while  $n$  is a combined variable, representing sodium channel inactivation as well as potassium activation. As the membrane voltage  $V$  spikes in time, the neuron's trajectory travels counter-clockwise around the phase plane (Fig. 3). The upswing and downswing of the action potential (dashed lines) correspond to the left-to-right and right-to-left trajectory jumps, respectively, between the arms of the  $V$ -nullcline (thick solid line). The  $V$ -nullcline and  $n$ -nullcline (fine solid line) correspond to points on the phase plane where  $dV/dt=0$  and  $dn/dt=0$ , respectively.

#### 3.2 The effect of increasing time scale separation

From the behavior of the trajectories of this two-variable ( $V$  and  $n$ ) model in the phase plane, we can relate the

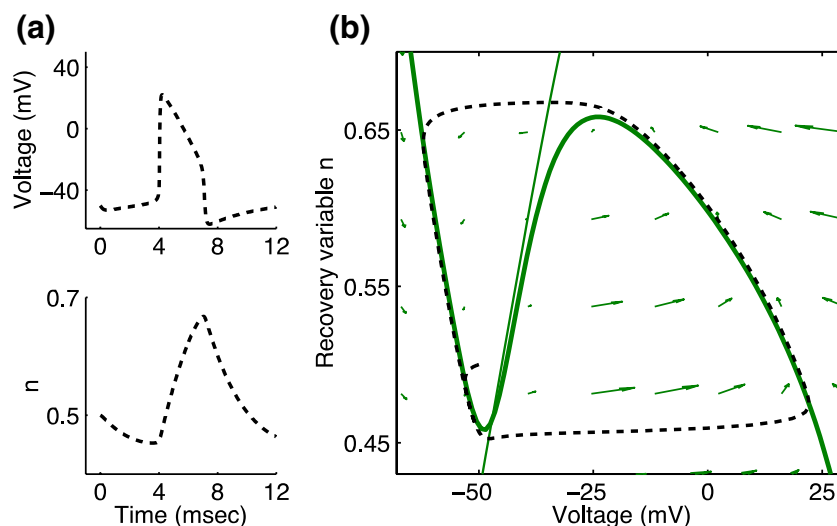


**Fig. 3** The action potential in the phase portrait. (a) The membrane voltage and recovery variable  $n$  change as a function of time and (b) can be plotted against each other in a phase portrait. The membrane voltage as a function of time shows a sharp upswing that corresponds to a rightward, horizontal movement in the 2D phase plane of voltage, the activation variable  $V$ , and the recovery variable  $n$ . Dashed lines

represent the neuron's trajectory, the N-shaped solid line is the  $V$ -nullcline, the solid straight line is the  $n$ -nullcline, and arrows represent the flow field with vectors given by  $(dV/dt, dn/dt)$  at each point  $(V, n)$ . Data are from the Type A model in Fig. 2 with stimulus mean  $I=50 \mu\text{A}/\text{cm}^2$

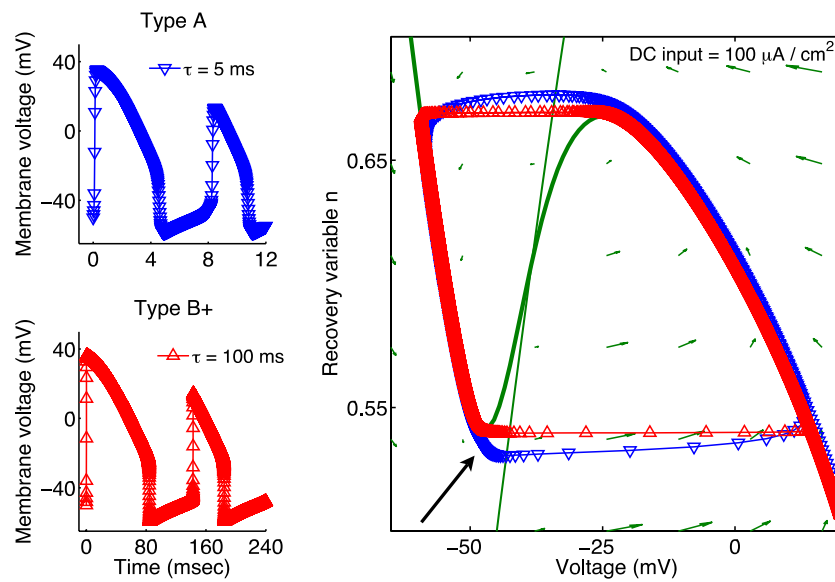


**Fig. 4** As the recovery time scale  $\tau$  increases, the upswing of the action potential (large, black arrow) occurs closer to the local minimum of the  $V$ -nullcline (curved green line). Changing the recovery time scale  $\tau$  does not alter the nullclines but rather affects how neuronal trajectories move in the phase plane, which can also be

seen in voltage vs. time plots (left; notice the different x-axis scale). The direction and magnitude of the small, green arrows represent the relative magnitudes of  $dV/dt$  and  $dn/dt$  for the  $(V, n)$  points in the phase portrait. Notice that trajectories overshoot the local minimum of the left arm of the  $V$ -nullcline (large arrow) only when  $\tau$  is small

computational behavior of the models to properties of the dynamical system. We considered two models that differed only in the value of the recovery variable time constant  $\tau$ : a short time scale model with  $\tau=5$  ms, and a model with  $\tau=100$  ms (see Methods). Figure 4 shows responses of both models to an input with a standard deviation of zero and an input mean of  $\mu=100 \mu\text{A}/\text{cm}^2$ . Without input fluctuations, the neuron spikes regularly with a stereotyped voltage trajectory. In other words, during the spike upswing the value of  $n$  is the same from spike to spike.

The time constant  $\tau$  controls the speed of the slow variable  $n$  in this model, while the speed of the fast variable  $V$  is governed by  $G_{\text{Na}}$ ,  $G_{\text{K}}$ , and  $G_{\text{Leak}}$ , biophysical conductance parameters describing the density of sodium, potassium, and leak channels in the membrane. Because the ionic conductances are constant,  $\tau$  represents the time scale separation in the model: as  $\tau$  increases, the time scale separation between the two variables increases. For increasing  $\tau$ , the spikes have a similar shape but are wider. Spikes of this width are clearly not physiological; this is a limitation of an increased time scale separation in 2D systems that we address later. The phase plane representation shows that as  $\tau$  decreases, trajectories start to overshoot the left and right bends of the  $V$ -nullcline (Fig. 4).

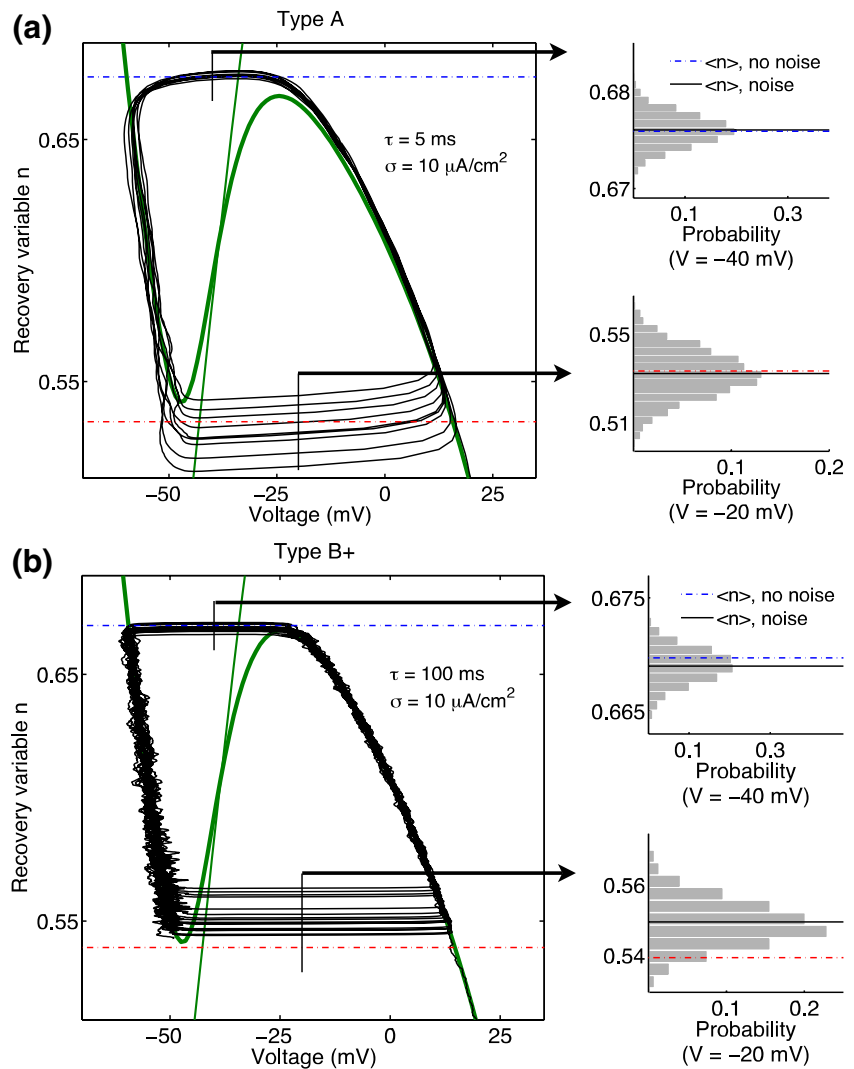
With a noisy input, voltage trajectories are less stereotyped and the intervals between spikes are irregular (Fig. 5). In the model with small  $\tau$ , noise does not change the mean value of  $n$  during spike upswings and downswings but only adds variability [Fig. 5(a)]. Thus, when there is little separation of time scales, input fluctuations do not alter

the mean firing rate, as seen in Fig. 2, but only spike timing. However, in the model with large  $\tau$ , input noise shortens the average oscillation period, increasing the mean firing rate [Fig. 5(b)]. Although noise does not appreciably change  $\langle n \rangle$  on the spike downswing, it does on average increase  $n$  during the upswing. When  $\tau$  is large, trajectories travel more slowly down the left arm of the  $V$ -nullcline. This allows input fluctuations the opportunity to initiate a spike sooner by pushing the neuron past its spiking threshold, which is approximately given by the upward-turning middle arm of the  $V$ -nullcline (Hong et al. 2007; Izhikevich 2007). Although this threshold is two-dimensional, once the neuron begins to fire,  $n$  stays relatively constant during the fast upswing of the action potential.

### 3.3 Defining an instantaneous potential barrier

Since noise causes the trajectory to jump across the threshold sooner, this implies that there is a barrier that prevents crossing in the absence of noise. To gain insight into how noise drives spiking, we examined how noise-driven trajectories escape over a barrier. Consider a simple 1D model as in Fig. 6(a), where input fluctuations of typical scale  $\sigma$  cause trajectories to move in the voltage  $V$  dimension, such that sometimes the trajectory can overcome an instantaneous potential barrier  $\Delta U$  located at a threshold for spiking. This picture is reminiscent of problems in physics and chemistry wherein the activation rate is determined by the size of an energy barrier and the temperature and is given by the Arrhenius rate or Kramer's

**Fig. 5** Input fluctuations do not change the mean firing rate when  $\tau$  is small, but increase firing rate when  $\tau$  is large. **(a)** When  $\tau$  is small (5 ms), input fluctuations ( $SD=10 \mu A/cm^2$ ) increase the variance of  $n$  during the up- and downswings of the action potential, but do not alter the mean value of  $n$ . Histograms are shown at right during action potential upswing ( $V=-20$  mV) and downswing ( $V=-40$  mV), as indicated by the vertical black lines on the phase portraits. The dashed lines represent the value of  $n$  when input  $SD=0$  mV, while the solid lines show the mean values of the data. The dashed and solid lines are nearly the same; the neuron’s firing rate does not change with increased input SD, but spiking becomes irregular. **(b)** When  $\tau$  is large (100 ms), increasing input SD leads to an increasing mean firing rate. Although the mean value of  $n$  during the action potential downswing does not appreciably change, during the upswing  $\langle n \rangle$  increases, since on average the input SD causes the neuron to spike sooner, i.e. before  $n$  has returned to the minimum. The input current  $I$  had a mean of  $100 \mu A/cm^2$



escape rate equation,  $r \sim \exp(-\Delta U/kT)$ . In our case, thermal energy  $kT$  is replaced by a factor proportional to the variance of the driving current fluctuations,  $\sigma^2$ .

DeVille et al. (2005) developed this framework for a Fitzhugh–Nagumo excitable system in the limit when noise  $\sigma$  is very small and  $\tau$  is very large. We wish to apply this approach to situations where the values of input noise  $\sigma$  and the separation of time scales  $\tau$  are relevant for physiological neurons. First, we test this relationship for less extreme values of  $\sigma$  and  $\tau$ .

To find  $\Delta U$ , we need the relevant potential. In general, the *potential* is defined as a scalar function with the property that its negative derivative is the force (Arfken and Weber 1995). When the separation of time scales is large, we can consider  $n$  to be fixed in the equation of motion for  $V$ , Eq. (5), so that the relevant force is  $-dV/dt$  and the problem reduces to a series of one-dimensional cases for various  $n$ . We therefore define the negative integral of  $dV/dt$  as an instantaneous potential landscape,

as in Fig. 6(a), for each value of  $n$ . Specifically, we consider:

$$\frac{dV}{dt} = \left( \begin{array}{l} -G_{Na}m_{\infty}^3(V)h(n)(V - E_{Na}) - G_Kn^4(V - E_K) \\ - G_{Leak}(V - E_{Leak}) + I \end{array} \right) / C, \tag{5}$$

which can be rewritten as:

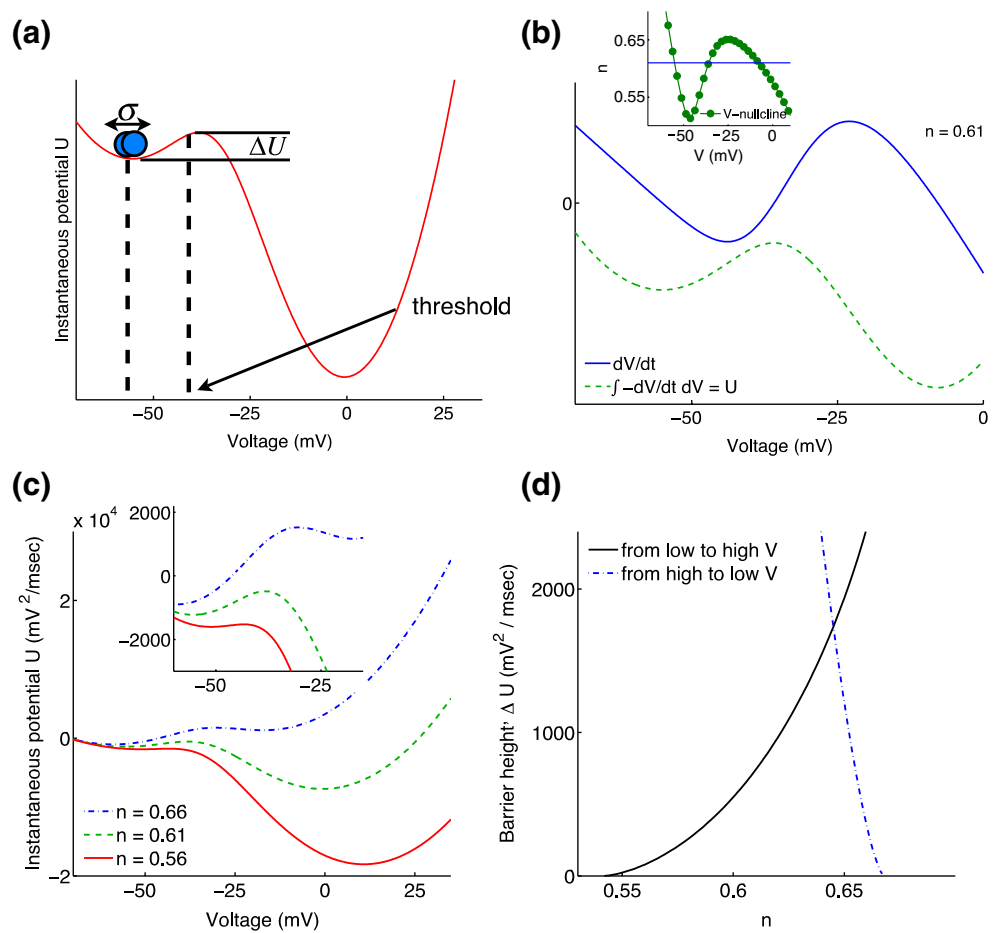
$$k_c = f(V, n), \tag{6}$$

where the  $k_c=0$  contour is the nullcline. As in DeVille et al. (2005), we seek a function  $U$  such that

$$\frac{\partial U(V, n)}{\partial V} = -f(V, n). \tag{7}$$

Integrating Eq. (6) with respect to  $V$ , we obtain  $U(V)$  for a given value of  $n$ . This produces a double-well potential

**Fig. 6** Input fluctuations can shorten interspike intervals by causing the neuron’s trajectory to cross an instantaneous potential barrier. **(a)** A simple 1D model relates spike initiation to crossing an energy barrier. **(b)** The instantaneous potential landscape can be found by integrating  $-dV/dt$  (solid, blue line) with respect to  $V$  for constant  $n$ , here represented by the solid black line in the inset. The result of the integral is represented by the dashed, green line. **(c)** The instantaneous potential landscape changes as  $n$  changes, and potentials are shown for three specific values of  $n$ , which represent three different slices through the inset of **(b)**. The action potential upswing and downswing occur at approximately  $n=0.56$  and  $n=0.66$ , respectively. The middle hump is the barrier related to the spiking threshold. Units are defined up to a constant. **(d)** The barrier height from low to high  $V$  is the potential  $U$  at the middle hump subtracted from the potential  $U$  for the left hump. As  $n$  increases, the barrier height for the rapid depolarization of the spike upswing increases



for each  $n$ , where the local minima and maxima of  $U(V)$  occur where the  $V$ -nullcline passes through that value of  $n$ . For an  $N$ -shaped nullcline, this leads to two minima and one maximum [Fig. 6(b)]. The shape of this instantaneous potential changes with  $n$ . During the spike upswing, the trajectory “rolls” down the potential to the right [Fig. 6(c, d), solid lines]. Then, as membrane voltages remain high,  $n$  increases until eventually the trajectory “rolls” down the potential to the left (Fig. 6(c, d), dash-dotted lines). When the separation of time scales is large, the potential landscape is quasistatic, and spikes can occur sooner due to noise-driven jumps over the potential barrier.

### 3.4 Relating $\tau$ and $\Delta U$

Given this expression for  $U$ , for every  $n$  there exists a barrier height  $\Delta U$ . By the Arrhenius, or Kramer’s escape rate, equation, the time scale  $\lambda(n)$ , or inverse rate, for jumping the barrier for a given input  $\sigma$  is given by:

$$\lambda(n) = k \exp(\Delta U(n)/m\sigma^2), \tag{8}$$

where  $m$  is a constant. As in DeVillie et al. (2005), for low noise levels the trajectory following a spike moves down

the left arm of the  $V$ -nullcline with a time scale determined by the recovery time constant  $\tau$ . While following this trajectory, the jumping rate  $\lambda^{-1}(n)$  changes with  $n$ . The system becomes susceptible to barrier crossing when  $\lambda(n)$  is of same order as the recovery time scale  $\tau$ . Therefore, we expect that average barrier crossing behavior of the system is characterized by

$$\tau = \langle k \exp(\Delta U(n)/m\sigma^2) \rangle, \tag{9}$$

where the brackets indicate an average over many spikes. Furthermore, since the variance of  $n$  at barrier crossing is small, and the value of  $n$  is nearly constant during each spike upswing and downswing, as seen in Fig. 5, we can simplify Eq. (9), without significant loss of accuracy, to:

$$\tau \cong k \exp(\Delta U(\langle n \rangle)/m\sigma^2). \tag{10}$$

$\Delta U(\langle n \rangle)$  is determined by evaluating the potential difference at  $\langle n \rangle$  for either the spike upswing (fast depolarization) or spike downswing (fast repolarization). If Eq. (10) accurately describes this system, we should find that  $\Delta U(\langle n \rangle)$  is linearly related to  $\ln(\tau)$ . Using the values of  $\langle n \rangle$  that correspond to a given  $\tau$  [Fig. 7(a)], we find that  $\Delta U$  and  $\tau$  are indeed exponentially related for a given  $\sigma$

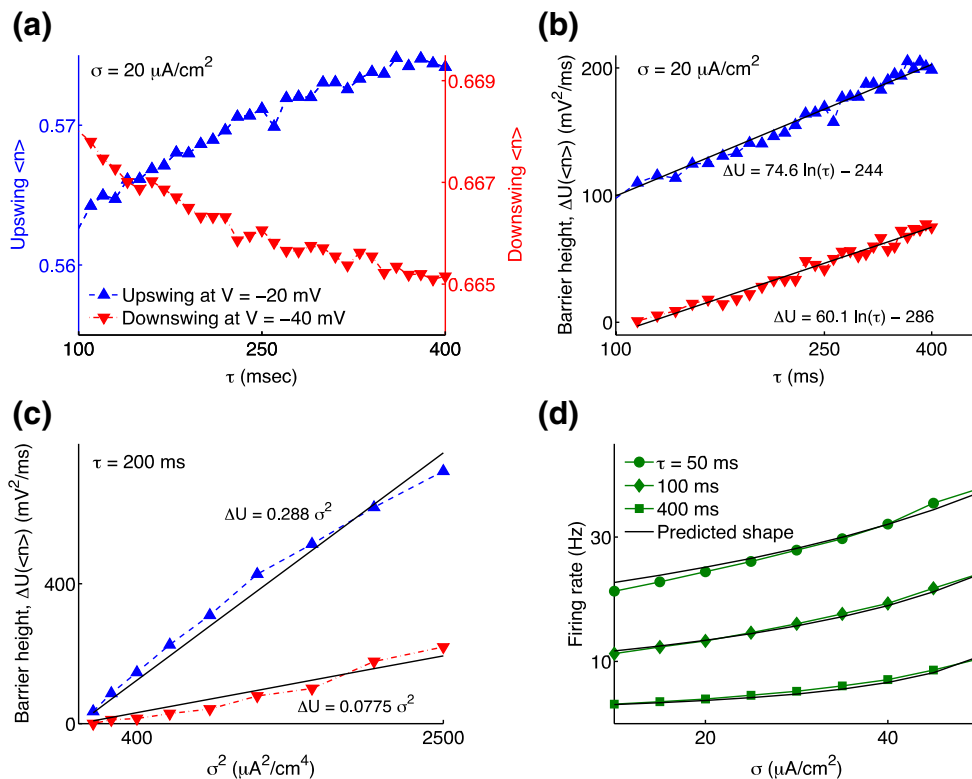


**Fig. 7** The ability of input fluctuations to cause an increase in firing rate is fit by an exponential relationship with the time scale separation. (a) As recovery time constant increases, action potentials are initiated and terminated sooner, i.e. upswings are at higher mean values  $\langle n \rangle$  and downswings are at lower  $\langle n \rangle$ . For each  $n$  there exists a barrier height  $\Delta U$ , as illustrated in Fig. 6. The upswing  $\langle n \rangle$  and downswing  $\langle n \rangle$  were measured at  $V = -20$  and  $V = -40$  mV, respectively, as in

[Fig. 7(b)], as suggested by the simple 1D picture of Fig. 6(a). The results in Fig. 7(b) and (c) can be summarized by the following equation:

$$\Delta U(\sigma, \tau) = (A \ln(\tau) + B)\sigma^2, \tag{11}$$

with  $A$  and  $B$  constant, and where  $\Delta U$  and constants differ for the upswing and downswing.

Thus, the simple picture of Fig. 6(a) holds approximately even away from the limits of very large time scale separation and low noise. We now wish to predict the mean firing rate as a function of  $\sigma$  and  $\tau$ . Equation (11) relates  $\sigma$  and  $\tau$  with  $\Delta U$ . We next relate the oscillation period  $T$  to  $n_{up}$ , the value of  $n$  when membrane voltage rapidly depolarizes during the spike upswing. Finally, we relate  $n_{up}$  to  $\Delta U$ .

We began by examining  $n$  and  $T$ . As seen in Fig. 4, for large  $\tau$  the trajectory spends essentially all of its time slowly moving along the left and right arms of the  $V$ -nullcline. Given this, one can find an approximate analytical expression for  $T(n)$  directly from the model equations. Along the

Fig. 5, and the symbols remain the same for the next two panels. (b) The mean barrier height  $\langle \Delta U \rangle$  is exponentially related to the separation of time scales, (c) and linearly related to input variance  $\sigma^2$ . (d) Firing rate increases with variance, as seen from simulation data (circles, diamonds, and squares). These firing rates can also be calculated as a function of  $\sigma$  with the parameter  $\tau = [50, 100, 400]$  ms using Eq. (15). The input current  $I$  had a mean of  $100 \mu A/cm^2$

$V$ -nullcline,  $dV/dt=0$ , and thus motion along the nullcline, i.e. along  $f(V, n)=0$ , can be described by dynamics due to  $dn/dt$ . In this case, the equation of motion is:

$$\tau \frac{dn}{dt} = n_{\infty}(V) - n.$$

The period of the trajectory, i.e. the interspike interval, is dominated by the time spent traveling on the left and right arms of the  $V$ -nullcline,

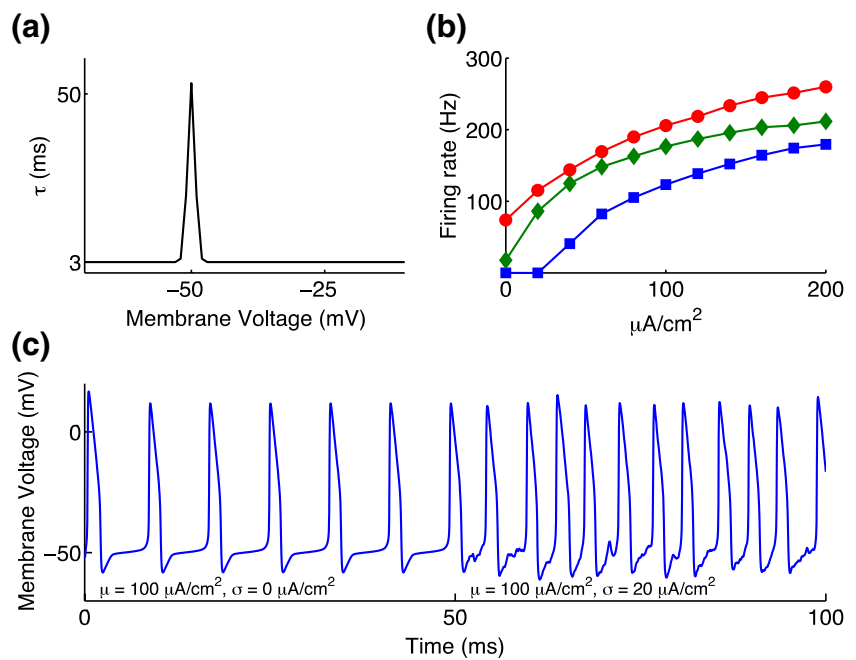
$$T = \tau \left( \int_L dn \left( \frac{1}{n_{\infty}(V) - n} \right) + \int_R dn \left( \frac{1}{n_{\infty}(V) - n} \right) \right), \tag{12}$$

where the bounds of integration are given by  $n_{up}$  and  $n_{down}$  for the left and right arms. One can numerically integrate Eq. (12) to find  $T(n_{up}, n_{down})$ .

We can, however, take a simpler approach based on the following observations. Due to the geometry of the nullclines, changes in  $n_{down}$  are small relative to those in



**Fig. 8** Addition of voltage dependence to the slow time scale of a 2D Hodgkin–Huxley model gives Type B+ behavior. (a) The time constant of the recovery variable is taken to be large only at peri-threshold voltages.  $C_{\text{Base}}=3$  ms,  $C_{\text{Amp}}=50$  ms,  $V_{\text{max}}=-50$  mV,  $\Delta=1$  mV (see Section 2). (b) This allows input fluctuations to increase average firing rate.  $SD=0, 10, 20 \mu\text{A}/\text{cm}^2$  for squares, diamonds, and circles, respectively. (c) Membrane voltages corresponding to two points on the  $f$ - $I$  curve as indicated. Spike widths are narrow



$n_{\text{up}}$  (Fig. 5), and the firing rate is relatively insensitive to  $n_{\text{down}}$ . We therefore consider only the dependence on  $n_{\text{up}}$ . Further, focusing on the left branch, the  $V$ -nullcline and the  $n$ -nullcline  $n_{\infty}(V)$  can be approximated as linear in this region, as suggested by the phase plots (e.g. Fig. 5). From the flow field, as depicted by the arrows in Figs. 3 and 4, it can be seen that the rate at which  $n$  changes with time decreases as the trajectory comes down the left branch. Thus, the time spent along the left branch is:

$$T_L = \tau \int_{n_{\text{down}}}^{n_{\text{up}}} \frac{1}{k_1 - k_2 n} dn = \tau \ln \left( \frac{k_1 - k_2 n_{\text{up}}}{k_1 - k_2 n_{\text{down}}} \right) = \tau \ln \left( 1 + \frac{(n_{\text{down}} - n_{\text{up}})}{k_1/k_2 - n_{\text{down}}} \right),$$

where  $k_1$  and  $k_2$  are positive constants and  $k_1 \gg k_2$ . A similar expression gives the time along the right branch. Using  $\ln(1+x) \approx x$  for small  $x$ , the oscillation time is approximated by

$$T \approx \tau(-\alpha n_{\text{up}} + \beta), \tag{13}$$

where  $n_{\text{down}} - n_{\text{up}}$  is small relative to  $n_{\text{down}}$  and  $\alpha$  and  $\beta$  are positive constants.

Now, we relate  $\Delta U$  and  $n$ . For the spiking barrier, i.e. for  $\Delta U_{\text{up}}$ , this is accomplished by finding  $V_1^*(n)$  and  $V_2^*(n)$ , the voltages for which  $dV/dt=0$  on the left and middle arms given  $n$ , and substituting them into  $U(V)$ , which is defined by Eq. (7). This gives  $\Delta U_{\text{up}} = U(V_2^*) - U(V_1^*)$  as in Fig. 6(d). In general,  $\Delta U_{\text{up}}(n)$  and  $\Delta U_{\text{down}}(n)$  are complicated functions that depend on the widths between the left and middle branches and right and middle branches of the  $V$ -nullcline, respectively. However, as can be seen from the

shape of the  $V$ -nullcline, they are monotonic, and numerically we find  $\sqrt{\Delta U(n)} \propto n$  to be a good approximation. We now have the necessary equations to calculate firing rate:

$$\begin{aligned} \Delta U &= (A_1 \ln \tau - B_1) \sigma^2 \\ \sqrt{\Delta U} &= A_2 n - B_2 \\ T &= (-A_3 n + B_3) \tau \end{aligned}, \tag{14}$$

where  $A_i$  and  $B_i$  are positive constants. Straightforward algebra yields an equation for the mean period,  $T$ :

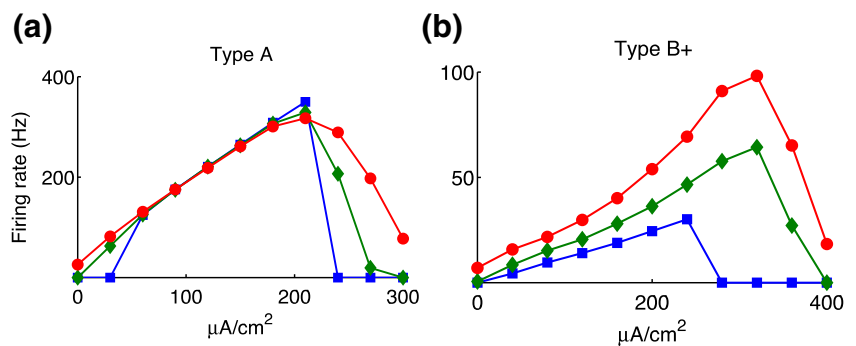
$$T = \tau \frac{-A_3}{A_2} \left( \sqrt{(A_1 \ln \tau - B_1) \sigma^2} + B_2 \right) + \tau B_3, \tag{15}$$

and thus  $T \propto (\text{const} - \sigma)$  for a given  $\tau$ . We find very good agreement between Eq. (15) and the simulated data [Fig. 7(d)].

### 3.5 Type B+ behavior with narrow spike widths

In this 2D model, large  $\tau$  leads to very wide spikes (e.g. Fig. 4), so this regime of a separation of time scales may seem physiologically irrelevant. To achieve B+ behavior with narrow spike widths in this model, one can manipulate the geometry of the nullclines around the left knee of the  $V$ -nullcline (Fig. 4, black arrow). For example, the model of Eq. (2) with  $k_m=5$  and  $k_n=23$  both has a sharper left knee of the  $V$ -nullcline and an  $n$ -nullcline that is reduced in slope, slowing spike trajectories at the left knee. This model exhibits Type B+ behavior with  $\tau=5$  ms and spike widths of approximately 5 ms. Increasing the dimensionality of the model is an alternative approach, allowing separation of the slow time constant from the spike recovery process. For example, one can add long time-scale adaptation through a

**Fig. 9** A Class I 2D Hodgkin–Huxley model can show either Type A or Type B+ behavior. The previous Class II model is now Class I (see Section 2) with (a)  $\tau=5$  ms, or (b)  $\tau=100$  ms.  $SD=0, 10, 20 \mu\text{A}/\text{cm}^2$  for squares, diamonds, and circles, respectively



slow spike-dependent current with a constant time constant, thus altering the shape of the  $V$ -nullcline as input current is increased.

Until now, we have considered the slow time constant of the recovery variable to be constant. However, a straightforward way to achieve narrow spikes in a 2D model is by allowing this time scale to be voltage dependent. When the recovery time constant becomes very large for peri-threshold voltages [Fig. 8(a)], spike trajectories slow down during depolarization, allowing the influence of noise. Thus, average firing rates become sensitive to input fluctuations [Fig. 8(b)], but spike widths are nonetheless narrow [Fig. 8(c)]. The details of the voltage dependence can strongly influence the details of shapes of the  $f$ - $I$  curves.

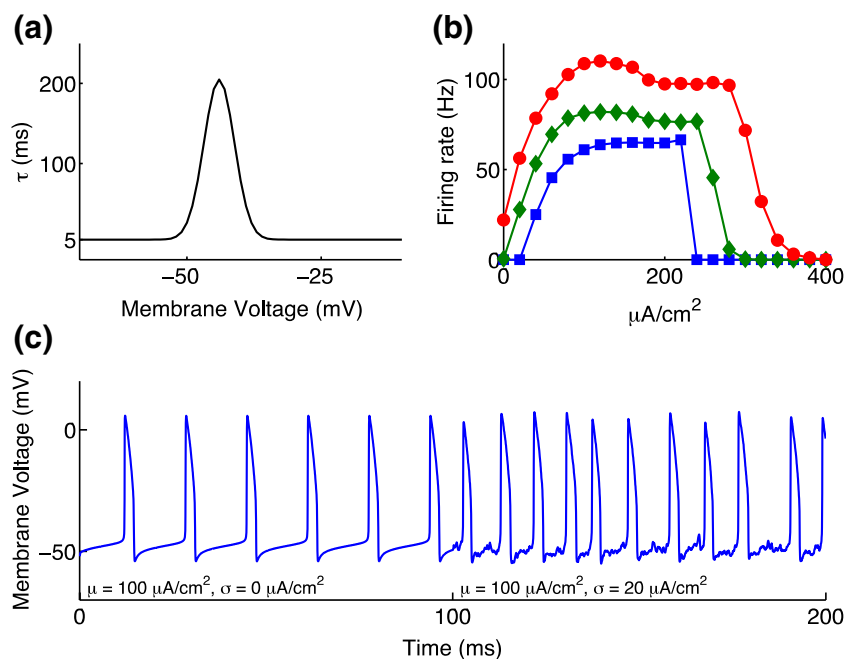
### 3.6 Relation to Hodgkin’s Classification

Our classification of neurons into types A and B is distinct from Hodgkin’s Class I/II/III categories (Hodgkin 1948). Hodgkin

classified neuronal response to noiseless injected current according to whether action potentials could be generated with an arbitrarily low frequency (Class I), with a certain minimum frequency with firing rates that were rather insensitive to applied current (Class II), or with only very strong current or not at all (Class III; Hodgkin 1948; Gerstner and Kistler 2002; Izhikevich 2007). This classification scheme focuses on how neurons respond to inputs in the absence of input fluctuations, and has been identified with the bifurcation structure of the neuronal dynamical system (Rinzel and Ermentrout 1998; Izhikevich 2007), while our approach emphasizes neuronal sensitivity to input fluctuations.

Although Type B– and Class III neurons are equivalent for excitable neurons (Hong et al. 2008; Lundstrom et al. 2008), there is no apparent correspondence between Classes I and II and Types A and B+. The 2D reduced HH models (Types A and B+) are Class II models, as verified by bifurcation analyses showing a loss of stability via a subcritical Hopf bifurcation. With the choice of parameters  $G_{\text{Leak}}=15 \text{ ms}/\text{cm}^2$ ,

**Fig. 10** Addition of a voltage-dependent slow time scale to a Class I 2D HH neuron model. (a) The time constant of the recovery variable is large only at peri-threshold voltages.  $C_{\text{Base}}=5 \text{ ms}$ ,  $C_{\text{Amp}}=200 \text{ ms}$ ,  $V_{\text{max}}=-44 \text{ mV}$ ,  $\Delta=4 \text{ mV}$  (see Section 2). (b)  $SD=0, 10, 20 \mu\text{A}/\text{cm}^2$  for squares, diamonds, and circles, respectively. (c) Membrane voltages corresponding to two points on the  $f$ - $I$  curve as indicated



$V_n = -30$  mV, and  $k_n = 5$ , the reduced models become Class I, Fig. 9. Their corresponding  $f-I$  curves are qualitatively identical to those of the Class II models, suggesting that the particular way in which the model loses stability does not dramatically influence its sensitivity to input fluctuations over its dynamic range. Similar results were obtained using the Morris-Lecar model (Morris and Lecar 1981) implemented with Class I dynamics (Rinzel and Ermentrout 1998; Tateno and Pakdaman 2004). This is in agreement with previous work showing that Class I and Class II Morris-Lecar models respond similarly to noisy inputs (Tateno and Pakdaman 2004), although other work has highlighted the models' different transient responses to fluctuating inputs near firing threshold (Gutkin and Ermentrout 1998; Robinson and Harsch 2002). As with the Class II models, adding voltage dependence to the recovery time constant of Class I neurons can give rise to Type B+ behavior. In Fig. 10, the time constant is larger for peri-threshold values, and the shape of the  $f-I$  curves depends on the particular form of voltage dependence, especially for inputs with large input fluctuations.

### 3.7 Higher dimensional models and adaptation

For these 2D models, a voltage-dependent recovery variable that slows greatly near threshold allows the neuron to be sensitive to input fluctuations while maintaining narrow spike widths. While in 2D models the time scales for voltage reset and for recovery from spiking are combined into a single variable, higher-dimensional models may have more than two time scales. Thus, slow recovery from sodium inactivation (Fleiderovich et al. 1996) may serve a similar function. In Fig. 11, we added a sodium inactivation gating variable to

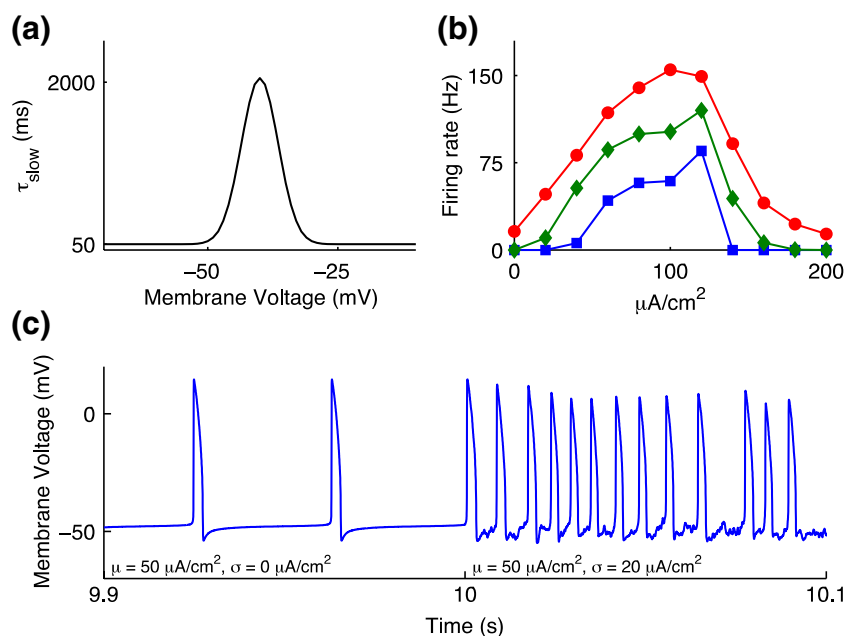
the Class I 2D HH model (see Section 2). This 3D model has three time scales: a fast time scale for membrane voltage, a slow time scale for the linearly related recovery variables  $n$  and  $h$ , and a yet slower, voltage-dependent time scale for the slow sodium inactivation variable  $s$ . This model also displays Type B+ behavior, over a wider parameter range than the 2D model of Fig. 10. The repolarization of spikes in Fig. 11(c) is governed by the intermediate time scale of  $n$  and  $h$ , while the slow depolarization just prior to spiking threshold is governed by the slowest time scale of  $s$ . When  $s$  has a fixed time constant, the effect of slow sodium inactivation in this model is to modify the shape of the  $V$ -nullcline differentially as firing rate increases; as for 2D models, this can also facilitate B+ behavior but the effect is not strong.

The important required effect is that the trajectories remain just below threshold for an extended time, allowing input fluctuations to initiate spiking sooner on average. For phase portraits such as Fig. 5, this corresponds to trajectories spending an extended time near the left knee of the  $V$ -nullcline. Lower energy barriers  $\Delta U$  occur when the system is held near threshold, and when there is a smaller distance between the left and center arms of the  $V$ -nullcline, Fig. 6. Thus, slow sodium inactivation, in addition to causing spike frequency adaptation (Fleiderovich et al. 1996), may facilitate sensitivity to input fluctuations as in Type B+ behavior.

## 4 Discussion

We set out to understand, using the simplest models possible, what is required to produce the experimentally observed

**Fig. 11** Addition of slow sodium inactivation to 2D HH neuron model. (a) The time constant of the slow sodium inactivation gate is large only at peri-threshold voltages.  $C_{\text{Base}} = 50$  ms,  $C_{\text{Amp}} = 2,000$  ms,  $V_{\text{max}} = -40$  mV,  $\Delta = 5$  mV (see Section 2). (b)  $SD = 0, 10, 20 \mu\text{A}/\text{cm}^2$  for squares, diamonds, and circles, respectively. (c) Membrane voltages corresponding to two points on the  $f-I$  curve as indicated. Slow depolarization near threshold voltages is controlled by slow sodium inactivation



diversity of  $f$ - $I$  curves in response to input mean and variance (Chance et al. 2002; Fellous et al. 2003; Rauch et al. 2003; Higgs et al. 2006; Arsiero et al. 2007), as in Fig. 1(a). Many single-compartment neuron models display converging  $f$ - $I$  curves and low sensitivity to input fluctuations at high input mean currents [Fig. 1(b)]; we call these Type A neurons. However, there are clear experimental examples of neurons whose  $f$ - $I$  curves show sensitivity to input fluctuations throughout their dynamic range [Fig. 1(a)], which we term Type B. Neuronal sensitivity to input fluctuations may provide an additional communication channel for neural coding (Fairhall et al. 2001), implement a type of noise-driven gain control (Chance et al. 2002; Higgs et al. 2006), underlie the ability of neurons to perform coincidence detection (Konig et al. 1996; Slee et al. 2005; Higgs et al. 2006), and promote persistent activity in networks (Arsiero et al. 2007). These computational regimes are distinct from Hodgkin's classification scheme; for example, a Type B neuron may be either Class I or II.

We parse Type B into two subtypes: B<sup>-</sup> and B<sup>+</sup>. B<sup>-</sup> neurons do not repetitively fire at steady state to noiseless current, regardless of how large, and are similar to differentiating neurons that respond primarily to input changes as seen in the auditory brainstem (Slee et al. 2005; Higgs et al. 2006). Previous work (Lundstrom et al. 2008) has explored the underlying causes of B<sup>-</sup> responses: these neurons always have a stable fixed point, meaning that input variance is an essential cause of spiking. Further, there is a well-defined boundary in conductance space between Type A and B<sup>-</sup>, such that upon lowering the conductance  $G_{Na}$ , a neuron can suddenly switch from Type A to B<sup>-</sup>. This boundary is planar in the 3D space of  $(G_{Na}, G_K, G_{Leak})$ , where an equation of the form  $G_{Na} - AG_K - BG_{Leak} = 0$  describes the boundary. The coefficients  $A$  and  $B$  can be determined analytically from model equations. Thus, it is a ratio of depolarizing and hyperpolarizing conductances that determines when a neuron is Type A or B<sup>-</sup>.

On the other hand, B<sup>+</sup> neurons can repetitively fire to noiseless current and are more similar to some cortical neurons (Rauch et al. 2003; Higgs et al. 2006; Arsiero et al. 2007). Here, we link Type B<sup>+</sup> behavior to two factors: the shape of the  $V$ -nullcline, which determines the height of an effective barrier to spiking, and a separation of time scales between an activation and recovery variable. Implicitly, the time scale of input fluctuations, which may be influenced by synaptic filtering and membrane time constants, must also be fast relative to that of the recovery variable. Our classification is based on sensitivity to input fluctuations, which is somewhat arbitrary. Here, we have classified neurons as sensitive to fluctuations, or Type B, when their firing rates vary by more than a few percent as input fluctuations are increased from zero to physiologically realistic levels (i.e. such that noise-induced membrane

voltage fluctuations are small compared to spike height). The transition from Type A to B for model neurons can be gradual, thus potentially creating difficulties with regard to classification. However, many *in vitro* and model neurons, as in Fig. 1, clearly fall into one of these types, emphasizing distinct differences in sensitivity to input fluctuations.

Although we initially focused on 2D systems, our results apply to 3D neuron models (Fig. 11), and thus may also be relevant for more complex experimentally recorded neurons. Slow sodium inactivation allows the voltage trajectory to stay near threshold for a prolonged amount of time, which gives rise to Type B<sup>+</sup> behavior. This may provide a theoretical underpinning for *in vitro* data showing Type B<sup>+</sup> behavior in response to somatically injected current Gaussian noise (Higgs et al. 2006; Arsiero et al. 2007). In these studies, slow adaptive mechanisms were implicated, both slow sodium inactivation (Arsiero et al. 2007) and slow afterhyperpolarization (sAHP) currents (Higgs et al. 2006), but the manner in which they were related to increased fluctuation sensitivity was unclear. For example, in Higgs et al. (2006) it was found that firing rates were more sensitive to input fluctuations in rat pyramidal neurons with large sAHP currents compared to those with small sAHP currents. With the application of  $\alpha$ -methyl-5-HT, a 5-HT<sub>2</sub> agonist that reduces sAHP currents, the sensitivity of the neurons to input fluctuations was reduced. When artificial sAHP currents were enhanced using dynamic clamp, the sensitivity of firing rates to input fluctuations was increased.

The present results more directly implicate adaptive mechanisms that have a voltage-dependent time constant that is large for peri-threshold values. However, in higher dimensional neurons it is possible that multiple time scales of currents active at peri-threshold voltages may interact such that slow currents with voltage-independent time constants also enhance fluctuation sensitivity. Certainly, in 3D models slow adaptive currents with voltage-independent time constants can alter the geometry of the  $V$ -nullcline such that trajectories are slower near threshold, although this has a weaker effect than a voltage-dependent recovery time constant.

In summary, we have categorized neurons into Types A, B<sup>+</sup>, and B<sup>-</sup> according to how the mean firing rate varies with input mean and variance. We identify three ways that a neuron might increase its sensitivity to input fluctuations: (1) by decreasing its effective sodium pool, or otherwise decreasing the inward-to-outward current ratio prior to spiking, so that the neuron's rest state is always stable (Lundstrom et al. 2008), (2) by changing conductances, or other parameters, to alter the shape of the  $V$ -nullcline, especially the width between the left and center arms that determines the barrier height  $\Delta U$ , and (3) by slowing a "recovery" time constant such that the neuron's voltage

spends a relatively long time near but below threshold. We believe that this analysis provides a simple and general picture of how the neuron's computation in terms of its  $f$ - $I$  curves depends on intrinsic parameters. These results help us better understand what from a biophysical standpoint determines or alters a neuron's input/output properties and may assist in predicting the functional effect of seemingly minor homeostatic or adaptive sub-cellular processes.

**Acknowledgments** We thank Bard Ermentrout for helpful conversations during initial stages of the project at the Marine Biological Laboratory's Methods in Computational Neuroscience 2007 course, Matthew Higgs and Michele Giugliano for helpful discussions and providing data for a figure, and Randy Powers and Sungho Hong for comments on a draft of this manuscript.

**Funding** This work was supported by a Burroughs-Wellcome Careers at the Scientific Interface grant and a McKnight Scholar Award; BNL was supported by grant number F30NS055650 from the National Institute of Neurological Disorders and Stroke, the Medical Scientist Training Program at UW supported by the National Institute of General Medical Sciences, and an ARCS fellowship; WJS was supported by a VA Merit Review.

**Author contributions** Conceived of, designed, and performed the simulations: BL. Analyzed the data: BL MF LS AF. Wrote the paper: BL MF WS AF. Developed the conceptual framework: BL MF LS WS AF.

## References

- Arfken, G. B., & Weber, H. -J. (1995). *Mathematical methods for physicists* (4th ed.). San Diego: Academic.
- Arsiero, M., Luscher, H. R., Lundstrom, B. N., & Giugliano, M. (2007). The impact of input fluctuations on the frequency-current relationships of layer 5 pyramidal neurons in the rat medial prefrontal cortex. *The Journal of Neuroscience*, *27*, 3274–3284. doi:10.1523/JNEUROSCI.4937-06.2007.
- Benda, J., Longtin, A., & Maler, L. (2005). Spike-frequency adaptation separates transient communication signals from background oscillations. *The Journal of Neuroscience*, *25*, 2312–2321. doi:10.1523/JNEUROSCI.4795-04.2005.
- Chance, F. S., Abbott, L. F., & Reyes, A. D. (2002). Gain modulation from background synaptic input. *Neuron*, *35*, 773–782. doi:10.1016/S0896-6273(02)00820-6.
- Connor, J. A., & Stevens, C. F. (1971). Prediction of repetitive firing behaviour from voltage clamp data on an isolated neurone soma. *The Journal of Physiology*, *213*, 31–53.
- Dayan, P., & Abbott, L. F. (2001). *Theoretical neuroscience : Computational and mathematical modeling of neural systems*. Cambridge, MA: Massachusetts Institute of Technology Press.
- Destexhe, A., Rudolph, M., Fellous, J. M., & Sejnowski, T. J. (2001). Fluctuating synaptic conductances recreate *in vivo*-like activity in neocortical neurons. *Neuroscience*, *107*, 13–24. doi:10.1016/S0306-4522(01)00344-X.
- Destexhe, A., Rudolph, M., & Pare, D. (2003). The high-conductance state of neocortical neurons *in vivo*. *Nature Reviews. Neuroscience*, *4*, 739–751. doi:10.1038/nrn1198.
- DeVille, R. E., Vanden-Eijnden, E., & Muratov, C. B. (2005). Two distinct mechanisms of coherence in randomly perturbed dynamical systems. *Physical Review E: Statistical, Nonlinear, and Soft Matter Physics*, *72*, 031105. doi:10.1103/PhysRevE.72.031105.
- Ermentrout, B. (1998). Linearization of F-I curves by adaptation. *Neural Computation*, *10*, 1721–1729. doi:10.1162/089976698300017106.
- Fairhall, A. L., Lewen, G. D., Bialek, W., & de Ruyter Van Steveninck, R. R. (2001). Efficiency and ambiguity in an adaptive neural code. *Nature*, *412*, 787–792. doi:10.1038/35090500.
- Fellous, J. M., Rudolph, M., Destexhe, A., & Sejnowski, T. J. (2003). Synaptic background noise controls the input/output characteristics of single cells in an *in vitro* model of *in vivo* activity. *Neuroscience*, *122*, 811–829. doi:10.1016/j.neuroscience.2003.08.027.
- Fleiderovich, I. A., Friedman, A., & Gutnick, M. J. (1996). Slow inactivation of Na<sup>+</sup> current and slow cumulative spike adaptation in mouse and guinea-pig neocortical neurones in slices. *The Journal of Physiology*, *493*(Pt 1), 83–97.
- Gerstner, W., & Kistler, W. M. (2002). *Spiking neuron models : Single neurons, populations, plasticity*. Cambridge, UK: Cambridge University Press.
- Gutkin, B. S., & Ermentrout, G. B. (1998). Dynamics of membrane excitability determine interspike interval variability: a link between spike generation mechanisms and cortical spike train statistics. *Neural Computation*, *10*, 1047–1065. doi:10.1162/089976698300017331.
- Higgs, M. H., Slee, S. J., & Spain, W. J. (2006). Diversity of gain modulation by noise in neocortical neurons: regulation by the slow afterhyperpolarization conductance. *The Journal of Neuroscience*, *26*, 8787–8799. doi:10.1523/JNEUROSCI.1792-06.2006.
- Hodgkin, A. L. (1948). The local electric changes associated with repetitive action in a non-medullated axon. *The Journal of Physiology*, *107*, 165–181.
- Hodgkin, A. L., & Huxley, A. F. (1952). A quantitative description of membrane current and its application to conduction and excitation in nerve. *The Journal of Physiology*, *117*, 500–544.
- Hong, S., Aguera y Arcas, B., & Fairhall, A. L. (2007). Single neuron computation: from dynamical system to feature detector. *Neural Computation*, *19*, 3133–3172. doi:10.1162/neco.2007.19.12.3133.
- Hong, S., Lundstrom, B. N., & Fairhall, A. L. (2008). Intrinsic gain modulation and adaptive neural coding. *PLoS Computational Biology*, *4*, e1000119. doi:10.1371/journal.pcbi.1000119.
- Izhikevich, E. M. (2007). *Dynamical systems in neuroscience : The geometry of excitability and bursting*. Cambridge, MA: MIT Press.
- Koch, C. (1999). *Biophysics of computation: information processing in single neurons*. New York: Oxford University Press.
- Konig, P., Engel, A. K., & Singer, W. (1996). Integrator or coincidence detector? The role of the cortical neuron revisited. *Trends in Neurosciences*, *19*, 130–137. doi:10.1016/S0166-2236(96)80019-1.
- Lundstrom, B. N., & Fairhall, A. L. (2006). Decoding stimulus variance from a distributional neural code of interspike intervals. *The Journal of Neuroscience*, *26*, 9030–9037. doi:10.1523/JNEUROSCI.0225-06.2006.
- Lundstrom, B. N., Hong, S., Higgs, M. H., & Fairhall, A. L. (2008). Two computational regimes of a single-compartment neuron separated by a planar boundary in conductance space. *Neural Comput*, *20*, 1239–1260.
- Moreno, R., de la Rocha, J., Renart, A., & Parga, N. (2002). Response of spiking neurons to correlated inputs. *Physical Review Letters*, *89*, 288101. doi:10.1103/PhysRevLett.89.288101.
- Morris, C., & Lecar, H. (1981). Voltage oscillations in the barnacle giant muscle fiber. *Biophysical Journal*, *35*, 193–213. doi:10.1016/S0006-3495(81)84782-0.
- Prescott, S. A., Ratte, S., De Koninck, Y., & Sejnowski, T. J. (2006). Nonlinear interaction between shunting and adapta-

- tion controls a switch between integration and coincidence detection in pyramidal neurons. *The Journal of Neuroscience*, 26, 9084–9097. doi:10.1523/JNEUROSCI.1388-06.2006.
- Rauch, A., La Camera, G., Luscher, H. R., Senn, W., & Fusi, S. (2003). Neocortical pyramidal cells respond as integrate-and-fire neurons to *in vivo*-like input currents. *Journal of Neurophysiology*, 90, 1598–1612. doi:10.1152/jn.00293.2003.
- Richardson, M. J. (2004). Effects of synaptic conductance on the voltage distribution and firing rate of spiking neurons. *Physical Review E: Statistical, Nonlinear, and Soft Matter Physics*, 69, 051918. doi:10.1103/PhysRevE.69.051918.
- Rinzel, J., & Ermentrout, B. (1998). *Analysis of neural excitability and oscillations*. In C. Koch, I. Segev, & (Eds.), (pp. 251–291, 2nd ed.). Cambridge, Massachusetts: MIT Press.
- Robinson, H. P., & Harsch, A. (2002). Stages of spike time variability during neuronal responses to transient inputs. *Physical Review E: Statistical, Nonlinear, and Soft Matter Physics*, 66, 061902. doi:10.1103/PhysRevE.66.061902.
- Rudolph, M., & Destexhe, A. (2005). An extended analytic expression for the membrane potential distribution of conductance-based synaptic noise. *Neural Computation*, 17, 2301–2315. doi:10.1162/0899766054796932.
- Rudolph, M., & Destexhe, A. (2006). On the use of analytical expressions for the voltage distribution to analyze intracellular recordings. *Neural Computation*, 18, 2917–2922. doi:10.1162/neco.2006.18.12.2917.
- Rush, M. E., & Rinzel, J. (1995). The potassium A-current, low firing rates and rebound excitation in Hodgkin–Huxley models. *Bulletin of Mathematical Biology*, 57, 899–929.
- Shadlen, M. N., & Newsome, W. T. (1994). Noise, neural codes and cortical organization. *Current Opinion in Neurobiology*, 4, 569–579. doi:10.1016/0959-4388(94)90059-0.
- Slee, S. J., Higgs, M. H., Fairhall, A. L., & Spain, W. J. (2005). Two-dimensional time coding in the auditory brainstem. *The Journal of Neuroscience*, 25, 9978–9988. doi:10.1523/JNEUROSCI.2666-05.2005.
- Strogatz, S. H. (1994). *Nonlinear dynamics and Chaos: with applications to physics, biology, chemistry, and engineering*. Reading, Mass.: Addison-Wesley.
- Tateno, T., & Pakdaman, K. (2004). Random dynamics of the Morris–Lecar neural model. *Chaos (Woodbury, N.Y.)*, 14, 511–530. doi:10.1063/1.1756118.
- VanRullen, R., Guyonneau, R., & Thorpe, S. J. (2005). Spike times make sense. *Trends in Neurosciences*, 28, 1–4. doi:10.1016/j.tins.2004.10.010.